

Effect of Relative Humidity on the Optimum Flute Shape for Corrugated Fiberboard

Thomas J. Urbanik
Research Engineer

U.S. Department of Agriculture
Forest Service
Forest Products Laboratory
Madison, Wisconsin

Abstract

Container stacking strength is an important performance requirement of corrugated fiberboard. The objective of this study is to examine theoretically how fluting geometry affects fiberboard strength and stiffness under standard relative humidity (RH) and high RH conditions. The fluted medium in a corrugated fiberboard is modeled as a connection of curved arc and straight flank segments passing through the middle plane of the cross section. Flute pitch, flute height, flank length, arc radius, and angle of wrap are reduced to a set of non-dimensional parameters, two of which can be chosen as independent. Thickness data on corrugated fiberboard in various flute profiles and weight grades are used to generate a set of representative flute profiles, which when combined further with mechanistic models on fiberboard edgewise crush strength and bending stiffness, enable strength and stiffness data from fiberboard to be used to predict average stress-strain properties of containerboard components. Using a standard set of papers as inputs, the strength and stiffness models are extrapolated to examine theoretically how mechanical properties and material savings are predicted to change for other arbitrary flute profiles. Predictions based on containerboard stress-strain properties at a standard 50% RH are compared with predictions based on stress-strain properties at 90% RH. The results quantify how an optimum flute profile strikes a balance among cost, runnability, strength, and stiffness considerations..

Introduction

Corrugated fiberboard has been used as a packaging material for at least one hundred years, a history on the evolution of corrugating machines being found in (Maltenfort, 1988). For earliest applications the wave shape, now called A-flute, of the fluted medium imparted a thick and soft cushioning ability to compete primarily with straw for packing fragile glass. Later a denser B-flute provided a better printing surface and more economy than A-flute per unit area of board. Then an intermediate size C-flute satisfied a compromise between performance and appearance. The ordering of flute sizes reflects their historical introduction.

Since its inception in 1936 by the National Motor Freight Traffic Association (NMFTA) of the American Trucking Association, Item 222 of the motor freight classification system for corrugated fiberboard containers has cited the applicability of the commonly used flute profiles. But in response to new practices in the containerboard industry, the NMFTA has de-emphasized attention to flute sizes to where, in 1996, Item 222 no longer makes any references to flute profiles. One cursory investigation by the Fiber Box Association found that one particular corrugating machine manufacturer was producing around fifty different profiles called C-flute. Performance requirements of corrugated fiberboard that reflect the updated distribution and handling practices are now motivating the design of custom profiles to match whatever linerboard and corrugating medium weight combinations the converter has available.

Container stacking strength is one important performance requirements and is a function of the edgewise compression strength and the bending stiffness of the corrugated fiberboard. The objective of this report is to examine theoretically how fluting geometry affects the fiberboard's strength and stiffness. This report augments our previous research that established theory on the optimum combinations of component thickness and stress-strain properties, for a fixed flute geometry, in corrugated fiberboard. In (Johnson, Urbanik, 1979) we derived a buckling theory of thin plate structures, appropriate to corrugated fiberboard, and set forth a rationale for distributing fiber between the linerboard and medium components, to obtain edgewise compression strength at a minimum weight. An example analyzed an A-flute profile with containerboard stress-strain properties fixed.

Subsequently in (Urbanik, 1981) we examined theoretically how changing the containerboard stress-strain properties affects the minimum weight design, again with the flute profile fixed. In this new report we consider the fluted geometry. The scope is limited to fixed containerboard weight grades and to fixed stress-strain properties. The collective principles of this current and our previous research can provide the basis for determining the optimum containerboard weight, stress-strain properties, and flute shape combinations.

Basic Geometry

The machined surface geometry of most corrugating rolls can be characterized by a sequence of arc sections connected by straight line tangents. The actual shape fabricated into the corrugated fiberboard is a complicated function of numerous process variables and the elastic interaction between paper components subjected to stretching and frictional forces. Previous researchers have sought to simplify the geometry and have advocated sinusoidal, elliptical, and trapezoidal shapes. But such shape functions tend to limit the accuracy in accounting for the true fluted length of the corrugated medium and the resulting cost.

Fortunately, the observed shape of defect free board is close enough to an arc-and-tangent profile to neglect a messy kinematic analysis, although such an analysis might be important to the equipment developer. The arc-and-tangent geometry proposed here is shown in Fig. 1. Flute pitch P , flute height H , and tip radius R dimensions are of the middle plane through the corrugated

medium, with top-to-bottom symmetry. The tip radius r and the root radius r' of the corrugating rolls differ by at least the caliper T_m of the corrugating medium. (In our discussions, caliper T is used to designate the surface-to-surface thickness. Later, effective thickness t is introduced to mean an equivalent thickness for dealing with stiffness effects.)

Arc-and-tangent corrugations have previously been analyzed for applications to metal roofing, siding, and drainage conduits. At first, moment of inertia calculations were of interest (Blodgett, 1934) but the calculations as presented depend on the graphical determination of various inputs. Wolford (Wolford, 1954) generalized the analysis and offered a set of closed form equations. Lou (Lou, et al., 1992) compared the arc-and-tangent geometry with sinusoidal and semi-elliptical models and added the fiberboard facings to derive a more general plate bending theory.

Our geometry as shown in Fig. 1 yields a set of equations with more general input parameters than those given in (Wolford, 1954) and is more applicable to corrugated fiberboard. Similarity between the two shaded triangles in Fig. 1 establishes the relationships

$$\frac{L}{R} = \frac{H - 2R(1 - \cos b)}{R \sin b} = \frac{P/2 - 2R \sin b}{R \cos b} \quad 1$$

where L is the length of the flank component in the model. The characterization is more readily obtained in terms of R instead of r and r' . The angle of wrap q is related to the half-angle $b = q/2$ as shown. The take-up-factor TF , defined as the ratio of the length of the unfluted corrugating medium to the length of the fluted geometry, is given by

$$TF = \frac{2L + 2Rq}{P} \quad 2$$

There is a benefit to expressing the basic geometry in terms of the non-dimensional parameters P/R , H/R , H/P , TF , and b , in that, given any two of these parameters, the remaining three are determinable from eqs. 1 and 2. A set of relationships among these parameters is given in Tables I and II. If P , H and R are known from the corrugating rolls, Table I can be used to determine b in terms of H/R and P/R , followed by the solution for TF in terms of b and either P/R , H/R , or H/P . Sometimes R is unknown, but P , H and TF , are determinable from the combined corrugated fiberboard. For this case, Table II gives solutions for b in terms of H/P , TF , and an estimated b for P/R in terms of b and TF , and for H/R . Note that b in Table II needs to be computed with successive iterations. Thus, an initial estimate, i.e., $b = 1$, yields an improved estimate, etc. until convergence.

In examining graphically the relationships among the various non-dimensional parameters, TF and q were chosen as the independent variables. Figure 2 shows contours of constant levels of H/P and contours of constant levels of P/R corresponding to variations in TF and q . Figure 2 was produced from the relationships given in Tables I and II over a range of interest typical of conventional corrugated fiberboard profiles. At a point (off the graph) where $P/R = 4$, $H/P = 0.5$, and $q = 180^\circ$ the geometry would consist of a connection of semicircular arcs without connecting flanks. As R approaches 0, P/R approaches infinity, and the geometry in the upper left corner of Fig. 2 approach an increasingly large triangular shape without arcs. Figure 2 readily shows what geometry must change to reduce TF , in order to reduce the amount and cost of corrugating medium for instance. Figure 3 shows contours of constant levels of H/R .

Typical flute profiles are given in Table III. These profiles were obtained by fitting our arc-and-tangent model to the caliper T_b data on combined corrugated fiberboard in (McKee, et. al. 1963) in combinations of four material grades and three flute sizes. A more complete discussion on this is given in the Appendix. In the analyses on choosing an optimum profile, as presented in the following sections of this report, the C-flute profile in Table III was used as a standard or reference profile.

Runnability

Before any flute profile can be considered, the corrugator must be able to run. An experimental study by (Hoke, Gottsching, 1983) examined the effect of the fluting geometry on the frequency of mechanical fractures occurring in the medium during corrugation. The researchers found that increasing q increases the frictional forces during corrugation and causes a higher frequency of fractures to occur in the flute flank. They also found that reducing r increases the bending stress around the flute tip in the medium and leads to more flute breaks at that point.

Predictions based on data (Hoke, Gottsching 1983) and applied to our standard profile are given in Fig. 4. The plot shows the frequency of corrugation breaks, relative to the frequency of breaks at the reference profile, for eight different profiles. The standard profile lies at the intersection of contour $H/P = 0.48$ and contour $P/R = 4.92$. Along the contour $H/P = 0.48$, H and P were fixed while R varied among four profiles, as indicated by the corresponding four points. Along the contour $P/R = 4.92$, P and R were fixed while H varied. Lastly, along the contour $H/R = 2.36$, H and R were fixed while P varied.

It can be inferred from Fig. 4 that geometry obtained by either reducing H or increasing P , while fixing R , reduces TF and the associated cost and also favorably reduces the frequency of corrugation breaks. In contrast, reducing R , while fixing P and H , to obtain a lower TF adversely increases the frequency of breaks.

Edge Crush Strength

The stress-strain properties of the linerboard and corrugated medium components comprising ten flute and grade combinations of corrugated fiberboard were predicted as described in the Appendix. Comparisons between the average experimental edgewise crush test (ECT) strength and the strength predictions based on those properties are given in Table AI therein. The nominal 205 g/m^2 (42 lb/1000 ft^2) facings, a nominal 127 g/m^2 (26 lb/1000 ft^2) corrugated medium, and their respective stress-strain properties representing the 1.38 MPa (200 lb—In this report units of lb instead of lb/in^2 are used for busting strength to be consistent with the original McKee, et.al., 1963 data.) series corrugated fiberboard components were considered as standard or reference paper properties and ECT strength was calculated for various fluting geometry.

The ECT strength of our standard profile comprised of our standard components is predicted (Table AI) to be 8.15 kN/m. Figure 5 shows contours of constant levels of ECT strength, normalized with respect to the ECT strength at the standard profile, for other TF and q combinations. The material properties and paper basis weights remain fixed for all profiles. For instance, at coordinates $TF = 1.48$ and $q = 124^\circ$, i.e., our standard C-flute profile, Fig. 5 shows that ECT strength differs by 0% from the standard condition, an obvious result. For the A-flute profile with $TF = 1.56$ and $q = 123^\circ$ (Table II) Fig. 5 shows that ECT strength differs by -4.9% from the standard condition. Compare this with the predicted ECT strength of 7.75 kN/m for the 200 lb, A-flute fiberboard in Table AI. In this manner Fig. 5 can be used to determine ECT strength for arbitrary flute profiles.

Figure 5 was produced with $R = 1.52$ mm but can be applied to other scales of geometry proportional to P , H , and R provided that the same material stress-strain properties prevail. To this end contours of constant levels of H/P are superimposed in Fig. 5. Note that the ECT strength of profiles in the upper left corner of Fig. 5 diminish to zero, i.e., a 100% strength reduction from the standard condition. This is because, with R fixed, as P and H approach infinity at those profiles, the local buckling strength of the corrugated fiberboard structure approaches zero.

Bending Stiffness

Bending stiffness EI data on the ten flute and grade combinations of corrugated fiberboard are given in Table AI of the Appendix. For a narrow corrugated fiberboard beam the EI is the sum of linerboard and corrugated medium EI components in the direction of bending as given by

$$EI = E_l J_l + E_m I_m \quad 3$$

in which E_l and E_m are the initial moduli of elasticity in the direction of strain of linerboard and medium material, respectively, and J_l and I_m , are the moment of inertia expressions for the combined linerboard facings and the fluted medium, respectively. Expressions for determining J_l and I_m are given in Table IV where they are normalized with respect to the combined board P and to either the linerboard caliper T_l or the medium caliper T_m . The expression for I_m is further divided in expressions I_f and I_t for the fluted flank and tip components, respectively.

As written, eq. 3 is applicable when bending occurs in the cross-machine direction CD, that is, when the flutes are aligned with the length of the beam. The I_m components in Table IV are relevant only to this case. With machine direction MD bending, the stiffness contributed by the fluted medium is negligible and the second term in eq. 3 can thus be ignored. Calculations of EI for the combined boards represented in Table AI revealed that the fluted medium contributes around 6%-13% to the total combined board stiffness, depending on the flute profile and grade.

The predicted EI levels in Table AI were determined for bending in the MD and the CD from the moment of inertia effects contributed only by the facings, i.e., $EI = E_l I_l$, which enabled us to estimate the extensional stiffness of facing material. Details on this are given in the Appendix. The EI of corrugated fiberboard with our standard profile and standard materials is predicted to be 14.04 Nm for MD bending and 5.92 Nm for CD bending (Table AI). The geometric mean stiffness $EI_{gm} = 9.12$ Nm. If the fluted medium is included, the more accurate $EI_{gm} = 10.2$ Nm.

Figure 6 shows contours of constant levels of EI_{gm} , normalized with respect to the EI_{gm} at the standard profile, for other TF and q combinations. Calculations are based on eq. 3. As in the case of the ECT calculations, the material properties and paper basis weights remain fixed for all profiles. For the A-flute profile with $TF = 1.56$ and $\theta = 123^\circ$ (Table II), for example, Fig. 6 shows that the EI_{gm} differs by 66% from the standard condition. To enable Fig. 6 to be used to determine the strength and stiffness benefits in changing the flute profile, contours of constant levels of ECT strength are superimposed.

Relative Humidity

The material properties reported on thus far were based on former experiments performed at 50 % RH. Additional stress-stress data acquired at 50% RH and at 90% RH (Gunderson, et. al., 1988) were examined for criteria that could be applied to our standard components to reflect how their properties would change if tested at 90% RH. Results are given in Table AIII of the Appendix as a second set of properties representing our standard components at 90% RH.

The analysis of edge crush strength and bending stiffness was repeated at the various TF and q combinations using the new material properties at 90% RH. Predictions of EI_{gm} with inputs at 90% RH were consistently around 57% of the EI_{gm} levels determined at 50% RH for all flute profiles. Thus, a change in RH appears to have little effect on the determination of the effect of the flute profile on bending stiffness.

The ECT strength of our standard profile comprised of our standard components with material properties at 90% RH is predicted to be 4.73 kN/m or 58% of the ECT strength predicted at 50% RH. Figure 7 shows contours of constant levels of ECT strength at 90% RH, normalized with respect to the strength at 50% RH for other TF and q combinations. For the profiles representing typical corrugated fiberboard geometry the ECT strength at 90% RH is around 57%-60% of the strength at 50% RH. Thus, again a change in RH appears to have little effect on the determination of the effect of the flute profile on edge crush strength. For profiles outside the range of those typically used (Fig. 7), the RH is seen to be more significant and should be considered in the design of novel flute profiles, for instance.

Summary and Conclusions

In this study an arc-and-tangent model is used to represent the geometry of the fluted medium in a corrugated fiberboard structure. Mechanical property data on corrugated fiberboard in various flute profiles and weight grades are used to derive a set of representative containerboard material properties. Mechanistic models of fiberboard edgewise compression strength and bending stiffness are manipulated to fit the data over the range of experimental profiles. Then, using a standard set of papers as inputs, these models are extrapolated to examine theoretically how performance and material savings are predicted to change for other arbitrary flute profiles. Predictions based on containerboard stress-stress properties at a standard 50% RH are compared with predictions based on stress-strain properties at 90% RH. The results quantify how an optimum flute profile strikes a balance among cost, runnability, strength, and stiffness considerations. The optimum flute profile depends to only a small amount on relative humidity.

Appendix

In the study by (McKee, et. al., 1963) nine companies supplied corrugated fiberboard material in combinations of three flute sizes and four weight grades (series). The averages of the caliper T_b , EI , and ECT strength data for each flute and series combination are repeated in Table A1. The basis weights BW correspond to the minimum carrier requirements for the combined weight of facings, as were in effect at the time of the study.

The variation of T_b with BW (Fig. A1) leads to predictions of H for each flute. From the y-axis intercepts we obtain, assuming parallel regression lines, $H+T_m = 4.81, 3.69,$ and 2.70 mm for A-, C-, and B-flute, respectively, and if the minimum carrier requirement for the corrugating medium that $T_m = 0.229$ mm is applied, these intercepts predict respective flute heights of $H = 4.57, 3.46,$ and 2.54 mm.

Take-up-factors for the A-, C-, and B-flutes, representing the industry in general, were reported to be 1.56, 1.42, and 1.36, respectively. The plots in Fig. A2 show how r varies with TF if the previous levels of H and T , are held fixed. Implicitly the plots yield H/R and thus P/R . If we represent all the flute profiles with a single $r = 1.41$ mm, which is consistent with the magnitudes reported in (Down, 1983), our model predicts levels of $P = 8.47, 7.21,$ and 6.35 mm for A-, C- and

B-flutes, respectively, which are within the industry's specified tolerances (Fiber Box Assoc., 1976). Flute geometry is summarized in Table III

Given the EI and the extensional stiffness Et of a laminate, an effective thickness $t = \sqrt{12EI / Et}$ yields the same modulus of elasticity E for both bending and extension. In general $t < T$ for paper. Substituting the expression for I_1 of combined board (Table IV) into EI of combined board and rearranging terms lead to the formula

$$EI \approx E_1 t_1 \left(\frac{(T_b - T_1)^2}{2} + \frac{T_1^2}{6} \right) = E_1 t_1 X \quad 4$$

in which X is the expression contained in parentheses. The first term of X accounts for facing extensional energy contributions to EI . The second term accounts for bending energy contributions. The approximation results from substituting T_1 for t_1 in the second term and from neglecting the corrugating medium.

Table AII gives the X -levels derived from the T_b and $H+T_m$ predictions. When the combined board EI - X data are plotted as shown in Figs. A3 and A4, it is readily established by eq. 4 that the slope of each regression line through each series of data is the average value of $E_1 t_1$ representing the series in the respective direction of bending. Combined board EI predictions from the regression lines are given in Table AI and the predicted facing $E_1 t_1$ -levels are given in Table AII.

In the plate structure model of (Johnson, Urbanik, 1989) ECT strength is determinable from t , width l , and stress-strain constants in the relationship $\sigma = c_1 \tanh(c^2 / c_1 E)$ for facing and medium micro plate elements as given in Table AIII. Facing and medium micro plate Z -dimensions are given by P and $P \cdot TF/2$, respectively. For facing elements, the stress-strain constant c^2 is given by $E_1 t_1 / t_1$ in the CD (Table AII) and A is the ratio of MD $E_1 t_1$ to CD $E_1 t_1$. Medium stress-strain properties were taken as the average of facing properties. An optimum value of $c_1 = 10.1$ MPa and optimum thickness functions of $t_1 = T_1 - 0.052$ mm for facing micro plates and $t_m = 0.229$ mm for medium micro plates were determined. Although numerous scenarios could obviously be found for optimizing the missing data, the optimization chosen herein was found to yield stress-strain curves and t -levels that are consistent with typical paper properties. ECT strength predictions are given in Table AI and compared with data in Fig. A5.

References

- Blodgett, H.B. 1934. Moment of inertia of corrugated sheets. *Civil Engr.*, 4(9): 492, 493, Sept.
- Down, A.G. 1983. The effect of flute profile changes on take-up ratio & medium cost. *Corrugator Rolls Workshop, Tappi Corrugated Containers Conference, Chicago, Oct.*
- Fiber Box Association. 1976. *Fiber Box Handbook*.
- Gunderson, D.E., J.M. Considine, and C.T. Scott. 1988. The compressive load-strain curve of paperboard: rate of load and humidity effects. *J. of Pulp and Paper Science*, Vol. 14, No. 2, pp. J37-J41, March.
- Hoke, U. and L. Gottsching. 1983. Physical technological characterization of the corrugating process part IIIb: Forming of corrugations as a function of profile geometry-assumptions and investigations. *Wochbl. Papierfabr.* 111, no. 7: 207-208, 210-212, 214; no. 8: 251-256, 258, April.
- Johnson, M.W., Jr, T. J. Urbanik, and W.E. Denniston. 1979. Optimum fiber distribution in singlewall corrugated fiberboard. *USDA, For. Serv. Res. Pap. FPL 348*.
- Johnson, M.W., Jr, and T.J. Urbanik. 1989. Analysis of the localized buckling in composite plate structures with application to determining the strength of corrugated fiberboard. *J. of Composites Tech. & Res.*, Vol. 11, No. 4, Winter, pp. 121-127.
- Luo, S., J.C. Suhling, J.M. Considine, and T.L. Laufenberg. 1992. The bending stiffness of corrugated board. *Mech. of Cellulosic Mtrls., ASME, AMD-Vol. 145/MD-Vol. 36*, pp. 15-26, Nov.
- Maltenfort, G.G. 1988. *Corrugated Shipping Containers: An Engineering Approach*. Jelmar Pub. Co., Inc., Plainview, NY.
- McKee, R.C., J.W. Gander, and J.R. Wachuta. 1963. Compression strength formula for corrugated boxes. *Paperboard Packaging*, 48(8): 149-159, August.
- Urbanik, T.J. 1981. Effect of paperboard stress-strain characteristics on strength of singlewall corrugated fiberboard: A theoretical approach. *USDA, For. Serv. Res. Pap. FPL 409*.
- Wolford, D.S. 1954. Sectional properties of corrugated sheets determined by formula. *Civil Engr.*, pp. 59, 60, Feb.

Table I—Relationships among non-dimensional parameters when P , H , and R are known	
Parameter	Equivalent Expression
β	$\tan^{-1}\left(\frac{4}{\sqrt{4(H/R)^2 - 16(H/R) + (P/R)^2}}\right) + \tan^{-1}\left(\frac{2(H/R) - 4}{P/R}\right)$
TF	$\frac{P/R - 4 \sin \beta}{(P/R) \cos \beta} + \frac{4\beta}{P/R}$
	$\frac{2 \cos \beta + 2\beta \sin \beta + H/R - 2}{(H/R - 2) \cos \beta + 2}$
	$\frac{(2\beta H/P - 1) \cos \beta - (\beta + 2H/P) \sin \beta + 1}{\cos \beta - 1}$

Table II—Relationships among non-dimensional parameters when P , H , and TF are known	
Parameter	Equivalent Expression
β	$\sin^{-1}\left(\frac{(2\beta(H/P) - TF - 1) \cos \beta + TF + 1}{\beta + 2(H/P)}\right)$
$\frac{P}{R}$	$\frac{4(\beta - \tan \beta)}{TF - \sec \beta}$
$\frac{H}{R}$	$\frac{H}{P} \frac{P}{R}$

Table III—Typical flute profiles.							
Flute	P	H	TF	H/P	P/R	H/R	θ
	Mm	mm					deg.
A	8.47	4.57	1.56	0.540	5.78	3.12	123
C	7.21	3.46	1.48	0.480	4.92	2.36	124
B	6.35	2.54	1.36	0.400	4.33	1.73	119

Table IV—Non-dimensional moment of inertia components.	
Term	Equivalent Expression
$\frac{I_1}{PT_1^3}$	$\frac{1}{2} \left(\frac{T_b}{T_1} - 1\right)^2 + \frac{1}{6}$
$\frac{I_t}{PT_m^3}$	$\frac{R}{P} \left(\left(4 \left(\frac{R}{T_m}\right)^2 + 1\right) \frac{\sin \theta + \theta}{4} + \left(12 \left(\frac{R}{T_m}\right)^2 + 1\right) \left(\frac{H}{R} - 2\right) \frac{\sin \beta}{3} + \left(\frac{R}{T_m}\right)^2 \left(\frac{H}{R} - 2\right)^2 \beta \right)$
x	$\frac{R}{T_m} \left(\frac{1}{2} \frac{P}{R} TF - \theta\right)$
$\frac{I_f}{PT_m^3}$	$\frac{1}{6} \frac{T_m}{P} (x^3 \sin^2 \beta + x \cos^2 \beta)$
$\frac{I_m}{PT_m^3}$	$\frac{I_t}{PT_m^3} + \frac{I_f}{PT_m^3}$

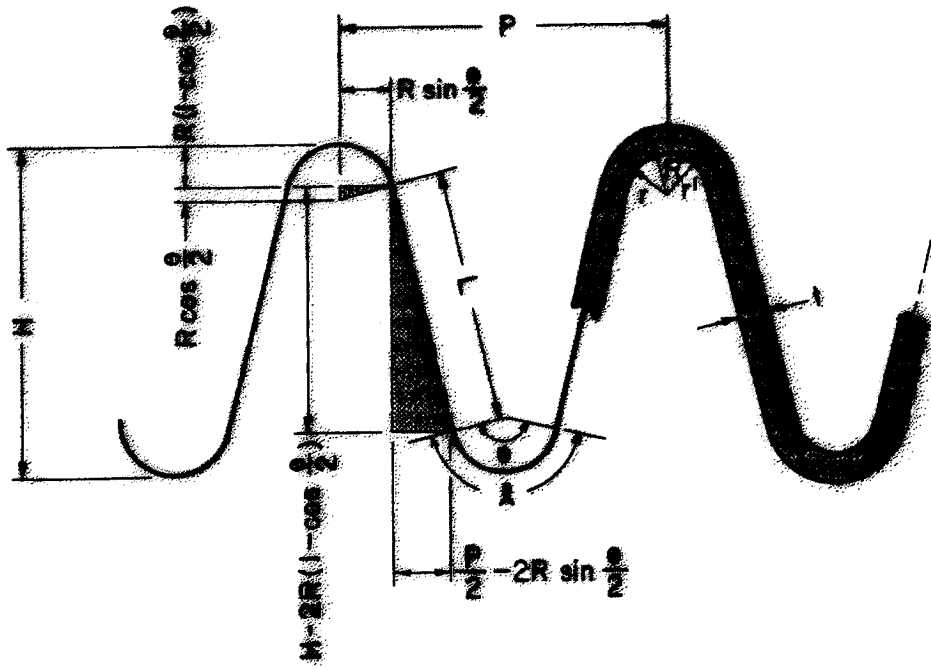


Figure 1 —Arc-and-tangent model through middle plane of corrugated medium.

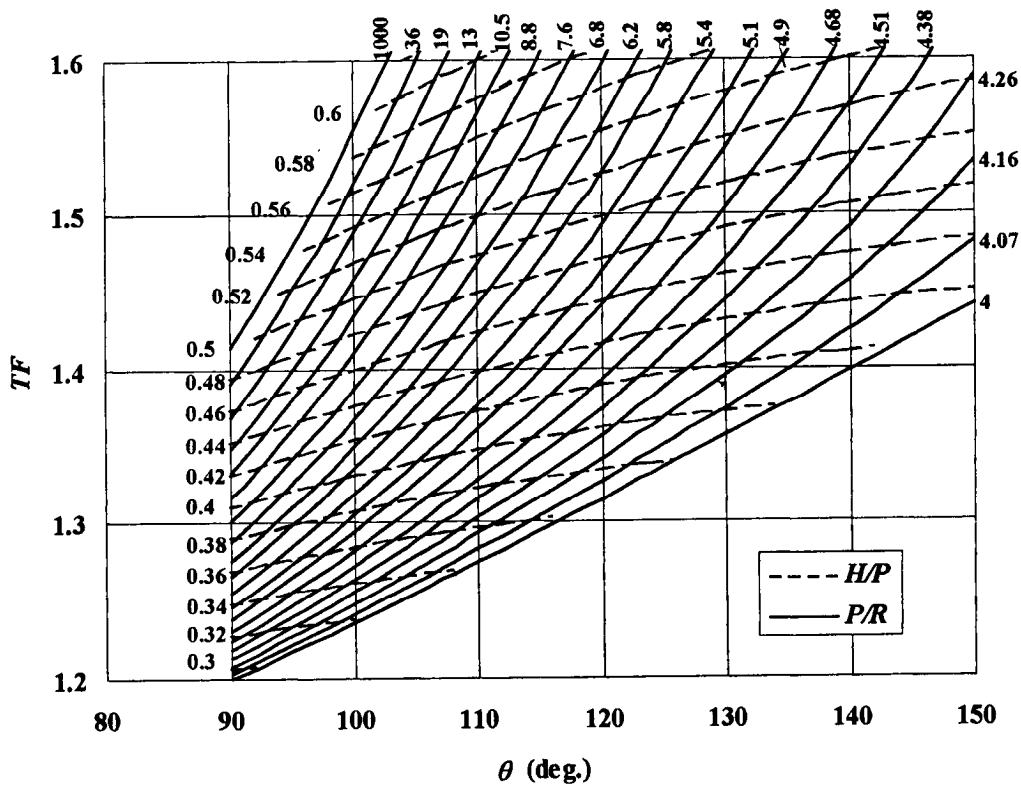


Figure 2 —Contours of constant levels of H/P and contours of constant levels of P/R corresponding to TF and q in arc-and-tangent model.

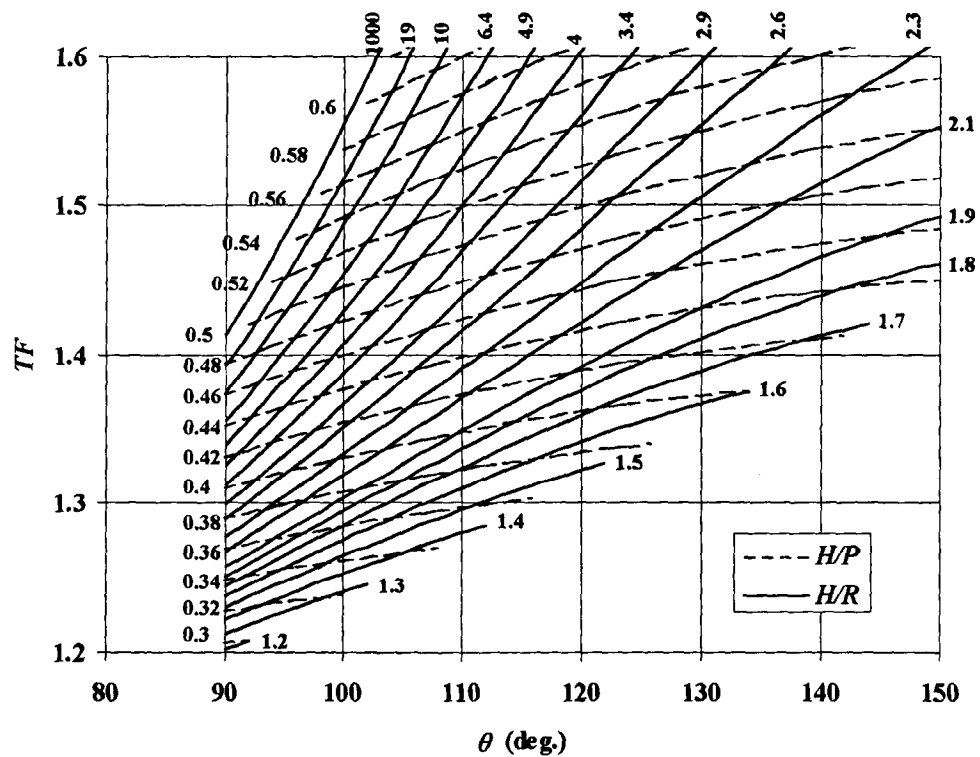


Figure 3 — Contours of constant levels of H/P and contours of constant levels of H/R corresponding to TF and q in arc-and-tangent model.

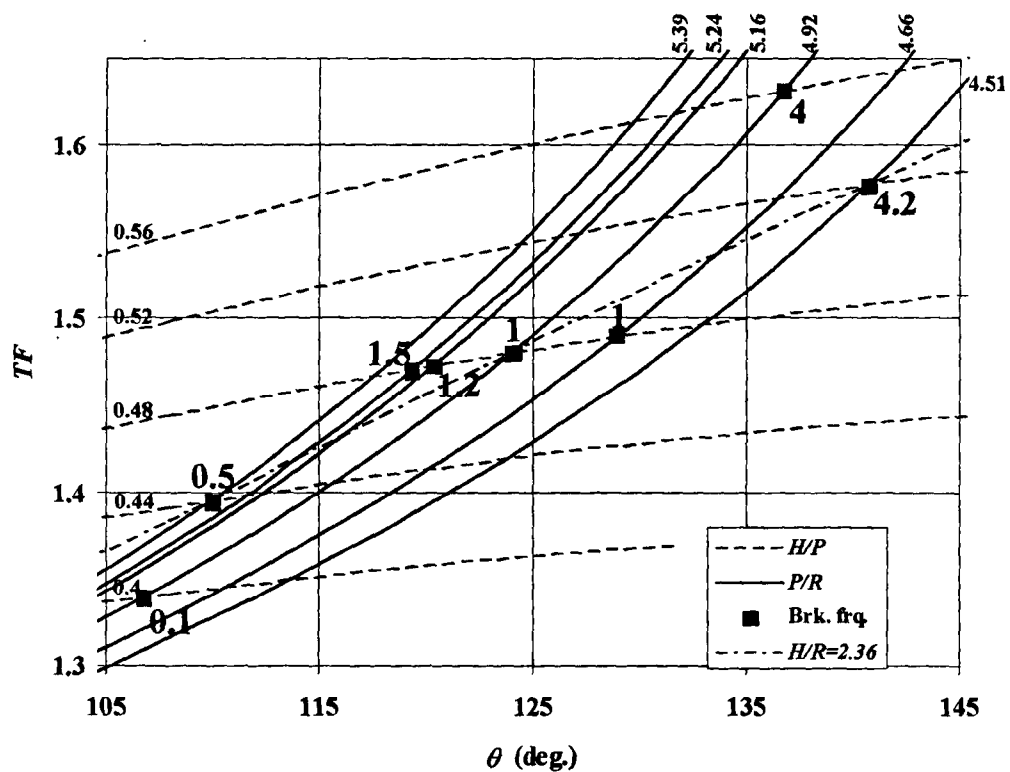


Figure 4 — Frequency of fractures occurring in corrugating medium, relative to frequency of fractures observed at a standard profile, for eight fluting profiles. Contours of constants levels of H/P , P/R , and H/R specify the profile geometry. The points correspond to eight specific profiles and the numbers correspond to their relative fracture frequencies.

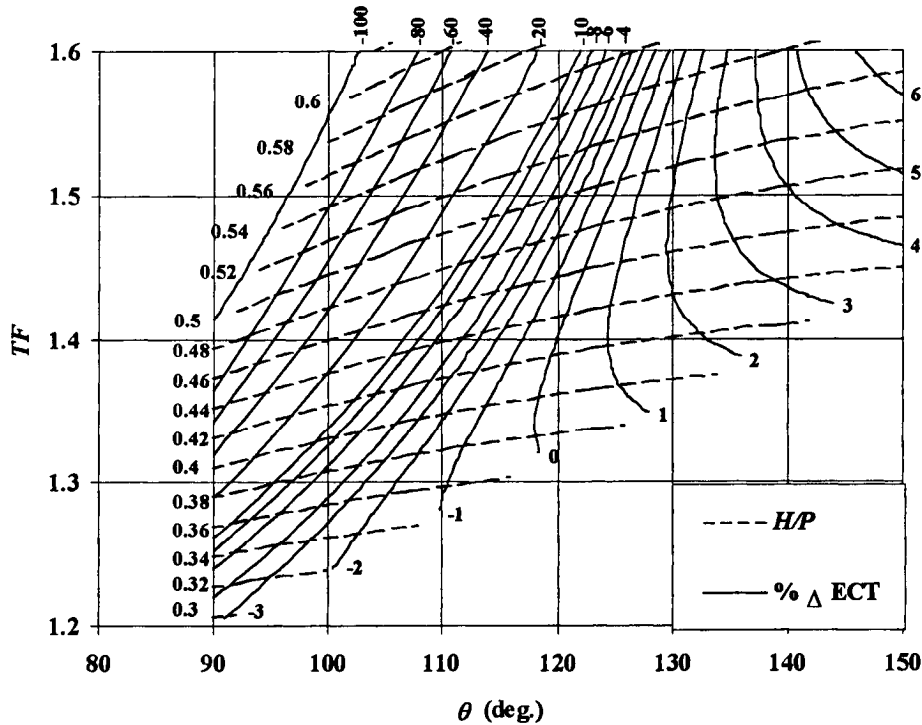
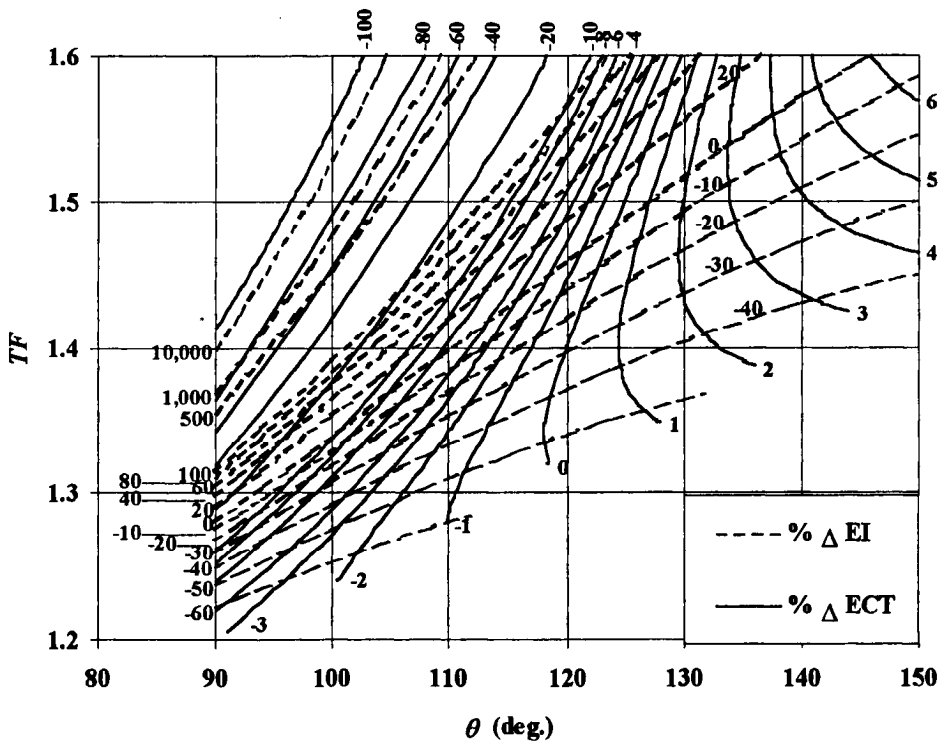


Figure 5 — Contours of constant levels of ECT strength (expressed as the % difference from a standard profile) and contours of constant levels of H/P . Linerboard and corrugated medium stress-strain properties are fixed at standard conditions and $R = 1.52$ mm in all the ECT calculations.

Figure 6 — Contours of constant levels of ECT strength and contours of constant levels of EI_{gm}



(ECT and EI_{gm} are expressed as the % difference from a standard profile). Linerboard and corrugated medium stress-strain properties are fixed at standard conditions and $R = 1.52$ mm in all the calculations.

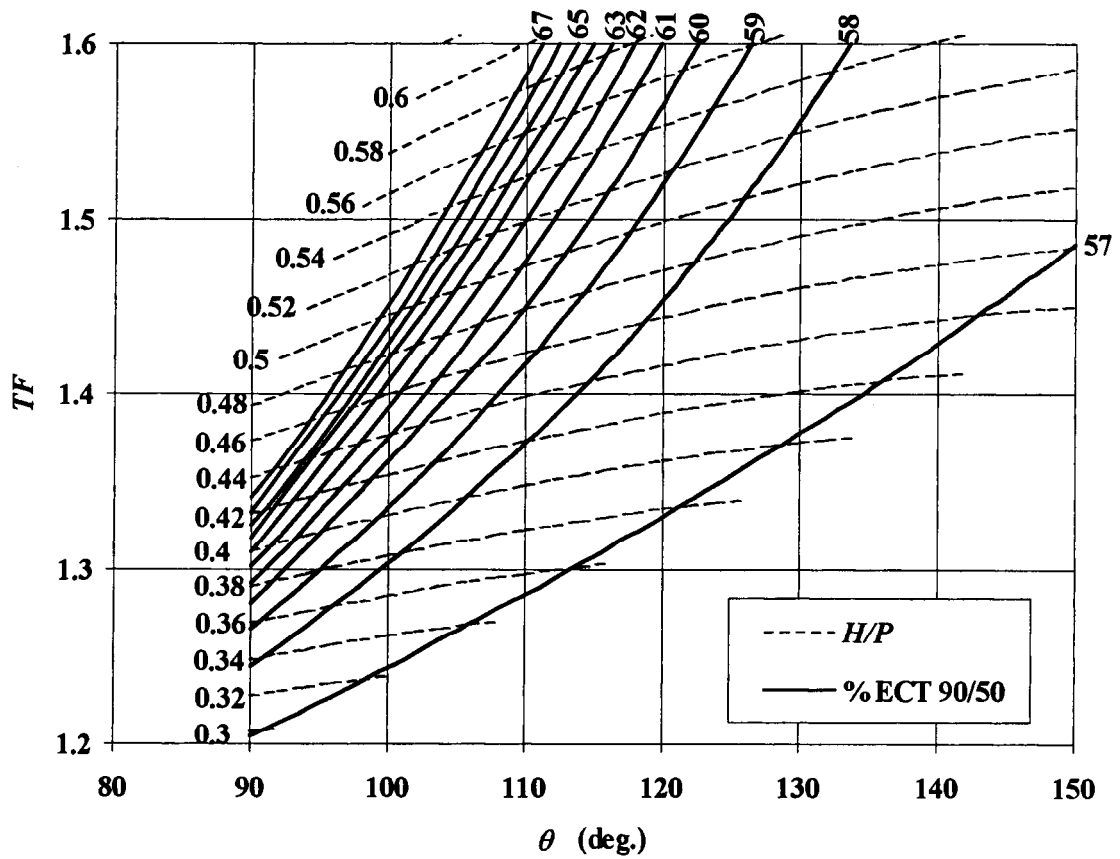


Figure 7 — Contours of constant levels of ECT strength (expressed as the percent of strength at 90% RH compared to the strength at 50% RH) and contours of constant levels of H/P . Linerboard and corrugated medium stress-strain properties are fixed and represent standard conditions adjusted for 90% RH. $R = 1.52$ mm in all the ECT calculations.

Flute Series BW		T_b			EI_{MD}			EI_{CD}			ECT			
		exp. pred. diff.			exp. pred. diff.			exp. pred. diff.			exp. pred. diff.			
lb	g/m ₂	mm	mm	%	Nm	Nm	%	Nm	Nm	%	kN/m	kN/m	%	
A	175	366	5.13	5.18	0.9	21.24	20.7	-2.3	9.08	9.09	0.0	7.29	7.06	-3.1
A	200	410	5.23	5.22	-0.2	22.71	23.1	1.9	9.72	9.76	0.5	7.92	7.75	-2.0
A	275	674	5.54	5.50	-0.7	28.81	30.5	5.9	15.93	16.1	1.3	10.53	11.09	5.3
C	175	366	4.14	4.07	-1.7	12.43	12.5	1.0	5.54	5.50	-0.7	7.43	7.53	1.4
C	200	410	4.06	4.11	1.2	14.91	14.0	-5.9	6.09	5.92	-2.8	7.72	8.15	5.6
C	275	674	4.52	4.39	-3.0	20.56	18.8	-8.6	10.06	9.94	-1.2	11.03	11.28	2.2
C	350	879	4.45	4.60	3.5	23.50	23.5	0.0	8.65	8.65	0.0	13.27	12.77	-3.8
B	175	366	3.02	3.15	4.1	6.15	7.30	18.8	3.13	3.20	2.1	7.60	7.59	-0.2
B	200	410	3.15	3.19	1.4	7.93	8.19	3.3	3.30	3.46	4.7	8.27	8.16	-1.3
B	275	674	3.63	3.46	-4.6	12.88	11.2	-13.0	6.27	5.93	-5.5	11.42	11.14	-2.5

Flute Series	e	T_b	$H+T$	T_1	X	$E_t I_1$	
						MD	CD
lb	mm	mm	mm	mm	mm ²	kN/m	kN/m
A	175	5.18	4.80	0.189	12.45	1667	729
A	200	5.22	4.80	0.212	12.57	1842	777
A	275	5.50	4.80	0.348	13.27	2299	1215
C	175	4.07	3.69	0.189	7.53	1667	729
C	200	4.11	3.69	0.212	7.62	1842	777
C	275	4.39	3.69	0.348	8.18	2299	1215
C	350	4.60	3.69	0.454	8.62	2725	1003
B	175	3.15	2.77	0.189	4.38	1667	729
B	200	3.19	2.77	0.212	4.45	1842	777
B	275	3.46	2.77	0.348	4.88	2299	1215

Table AIII—ECT plate element properties at 50% RH, except where noted. (Properties in parentheses are estimated values at 90% RH.)											
		Facing					Medium				
Flute Series	lb	<i>t</i>	<i>l</i>	<i>c</i> ₁	<i>c</i> ₂	<i>A</i>	<i>t</i>	<i>l</i>	<i>c</i> ₁	<i>c</i> ₂	<i>A</i>
		mm	mm	MPa	GPa		mm	mm	MPa	GPa	
A	175	0.241	8.47	10.1	3.02	2.28	0.229	6.61	10.1	2.90	2.24
A	200	0.264	8.47	10.1	2.94	2.37	0.229	6.61	10.1	2.90	2.24
A	275	0.400	8.47	10.1	3.03	1.89	0.229	6.61	10.1	2.90	2.24
C	175	0.241	7.21	10.1	3.02	2.28	0.229	5.33	10.1	2.90	2.24
C	200	0.264	7.21	10.1	2.94	2.37	0.229	5.33	10.1	2.90	2.24
C	200	0.264	7.21	(5.69)	(2.00)	(2.73)	0.229	5.33	(5.62)	(1.90)	(2.18)
C	275	0.400	7.21	10.1	3.03	1.89	0.229	5.33	10.1	2.90	2.24
C	350	0.506	7.21	10.1	1.98	2.72	0.229	5.33	10.1	2.90	2.24
B	175	0.241	6.35	10.1	3.02	2.28	0.229	4.32	10.1	2.90	2.24
B	200	0.264	6.35	10.1	2.94	2.37	0.229	4.32	10.1	2.90	2.24
B	275	0.400	6.35	10.1	3.03	1.89	0.229	4.32	10.1	2.90	2.24

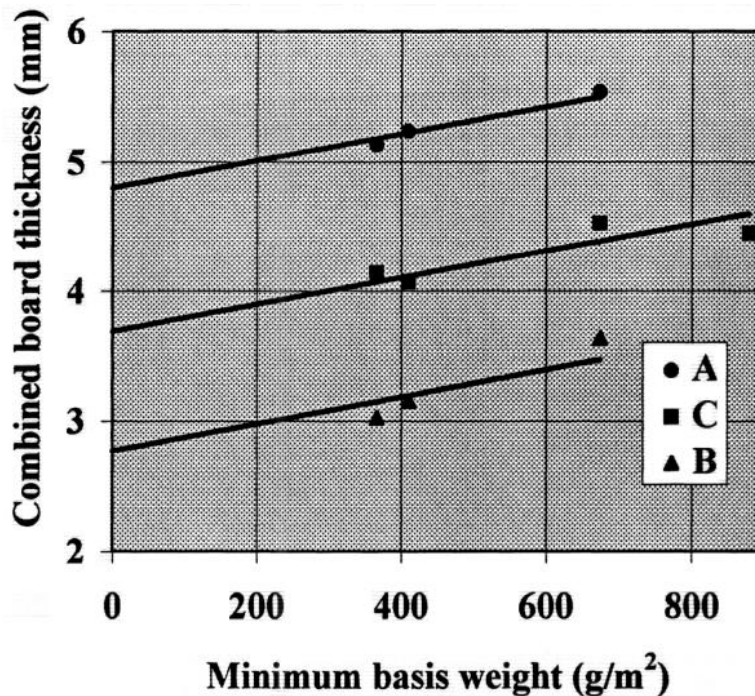


Figure A1 — Variation of the average caliper T_b of combined corrugated fiberboard with the minimum combined facing basis weight required at the time of the study. The points are average T_b -levels for three flute sizes from (Mckee, et. al., 1963) and the lines are regression parallels.

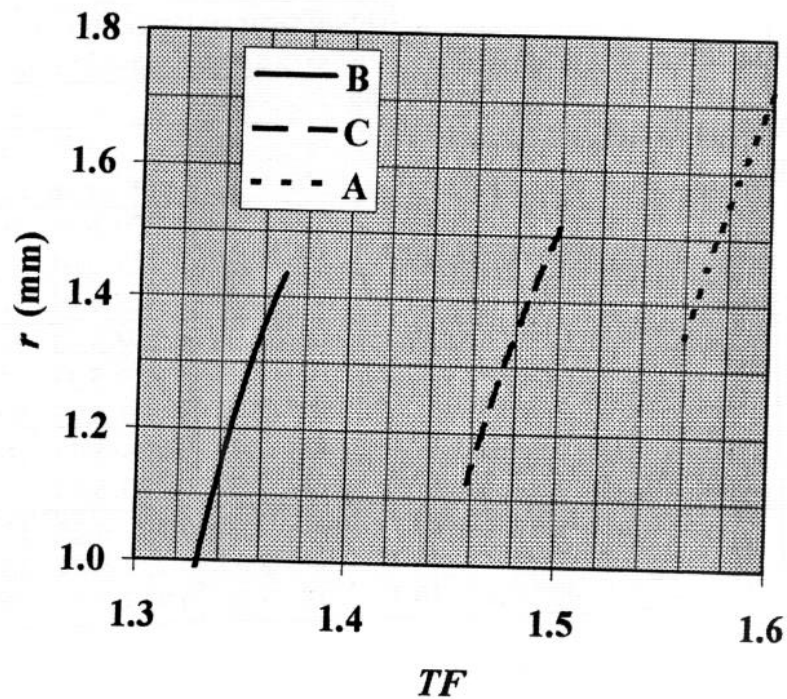


Figure A2 — Variation of the radius of curvature r of the fluting roll flute tip with the combined board take-up-factor TF when the flute height $H = 4.57, 3.46,$ and 2.54 mm, corresponding to A-, C-, and B-flute profiles, respectively, and the corrugated medium caliper $T_m = 0.229$ mm.

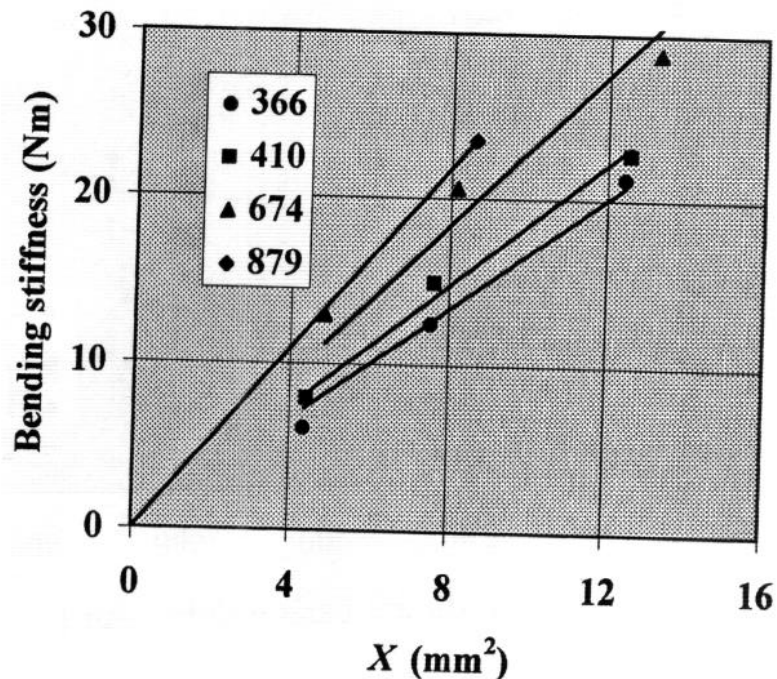


Figure A3 — Variation of the bending stiffness of combined corrugated fiberboard in the machine direction (MD) with parameter X from eq. 4. The points are data from 3 flute sizes and 4 combined basis weights (BW) of facing material in g/m^2 . The lines are regressions through the origin. The slope of each line through data for each BW is the linerboard extensional stiffness in the MD.

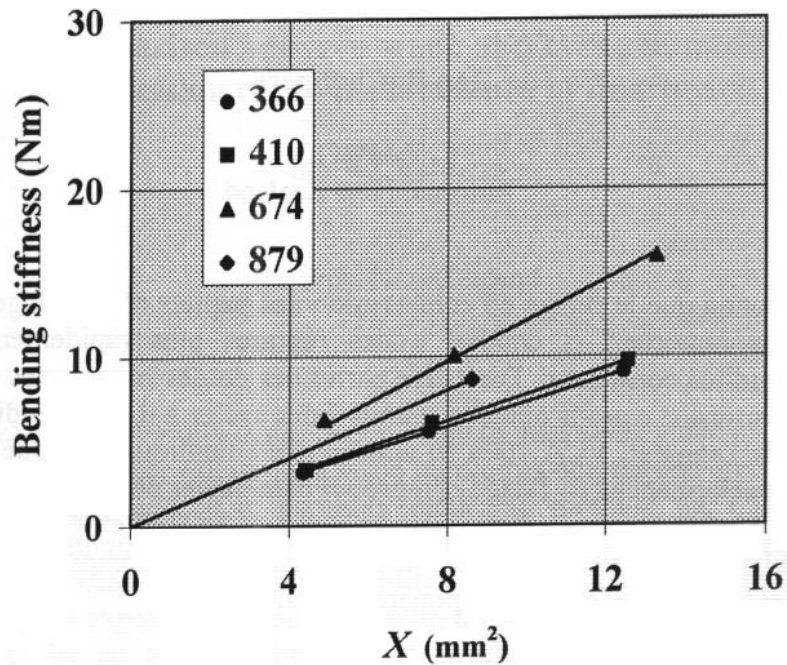


Figure A4 — Variation of the bending stiffness of combined corrugated fiberboard in the cross machine direction (CD) with parameter X from eq. 4. The points are data from 3 flute sizes and 4 combined basis weights (BW) of facing material in g/m^2 . The lines are regressions through the origin. The slope of each line through data for each BW is the linerboard extensional stiffness in the CD.

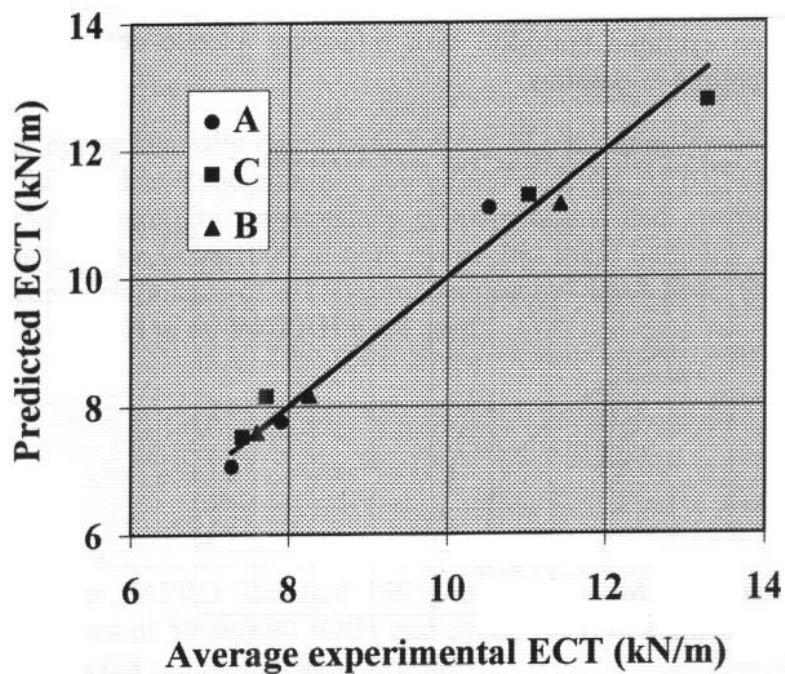


Figure A5 — Comparison between ECT strength predictions, based on an optimum set of containerboard stress-strain properties, and data for 3 flute sizes.